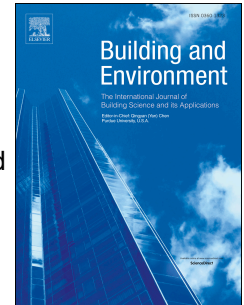# Accepted Manuscript

Effect of overhang on wind-driven rain wetting of facades on a mid-rise building: Field measurements

Hua Ge, Vincent Chiu, Ted Stathopoulos

Please cite this article as: Ge H, Chiu V, Stathopoulos T, Effect of overhang on wind-driven rain wetting of facades on a mid-rise building: Field measurements, *Building and Environment* (2017), doi: 10.1016/j.buildenv.2017.03.034.

Effect of overhang on wind-driven rain wetting of facades on a mid-rise building: field measurements

Hua Ge[*1], Vincent Chiu[2] and Ted Stathopoulos[3]

[*]Corresponding author: Dr. Hua Ge, hua.ge@concordia.ca, 1-514-848-2424 ext. 8771

Address: 1455 de Maisonneuve, Montreal, Quebec, H3G 1M8

[1]Associate Professor, Department of Building, Civil and Environmental Engineering
Concordia University, Montreal, Quebec, Canada

[2] Building Science Specialist, ROXUL Inc., Milton, Ontario, L9T 6W3

[3] Professor, Department of Building, Civil and Environmental Engineering, Concordia
University, Montreal, Quebec, Canada

1

Abstract

Wind-driven rain (WDR) is one of the main sources of moisture damages in buildings. Roof overhangs are a common feature that can be used to reduce WDR on building facades. However, there is very limited information on the quantitative evaluation of the effectiveness of overhangs in reducing WDR on building façades, especially through field measurements. A six-story building with a low-sloped roof located in Vancouver has been equipped with a retractable overhang along with a rooftop weather station measuring wind speed, wind direction and horizontal rainfall and a total of 31 WDR gauges measuring WDR on building facades. The spatial distribution of WDR on the building façade has been studied without and with overhangs. The effectiveness of roof overhang is studied with respect to wind speed, wind direction and rainfall intensity. Field measurements show that for the particular climate characterized by long rainy winters with mild wind and rain, the overhang is effective and significantly reduces WDR for this six-story building, especially for areas directly underneath the overhang. The protection increases from the side edge to the center and from the bottom to the top of the façade. As expected, the larger overhang provides greater protection. The relationship between overhang effectiveness and distance from the roofline is quasi-linear with smaller gradient for the larger overhang. The effectiveness of the overhang is highly dependent on wind speed and wind direction - it increases for oblique winds but decreases with the increase of wind speed.

Keywords: Wind-driven rain (WDR), field measurements, effectiveness of overhang, building façades

1. INTRODUCTION

Wind-driven rain (WDR) is one of the most important environmental loads and the main moisture source that affects the hygrothermal performance and durability of building envelopes [1]. Wind-driven rain, the amount of rainwater that impinges on the vertical surface of building envelopes under the influence of wind, is the result of complex interactions among wind, rain and buildings. The quantity and spatial distribution of WDR is affected by a wide range of parameters including wind speed, wind direction, rainfall intensity, building geometry, location on building facades, and surrounding topography. WDR loads are normally determined or estimated by measurements, semi-empirical correlations, and Computational Fluid Dynamics (CFD) modelling; and each approach has its own advantages and limitations [2]. The importance of WDR has led to research efforts in the past [3-12]. In recent years, the application of advanced numerical modelling [13-20] and efforts in collecting high quality and high resolution measurements [21-24] have advanced our understanding of this complex phenomenon such as the effect of building size, configurations and geometrical details, local weather conditions [25-32], and turbulence dispersion [33-36].

Roof overhangs have been traditionally used for several purposes including protection against rain. Previous studies show that the shapes of roofs and overhangs have a significant impact on the amount of WDR deposited on building façades. Pitched roofs and overhangs protect the walls below them by shadowing and redirecting airflow. Inculet and Surry [37] studied the influence of building geometry and architectural details such as balconies, cornices, pitched roofs, and inset corners on the wetting pattern of scaled down building models placed in a boundary layer wind tunnel. They found that cornices may be successful in protecting the top of the building façade just below the cornice. Blocken and Carmeliet [13] performed WDR measurements on a low-rise building with a combination of a flat-roof and a sloped-roof with different overhang widths. Their study found that the flat roof with a smaller overhang width received significantly more rain than the sloped roof with a slightly larger overhang. Field observations have shown that roof overhangs are effective under certain climates. For example, the field survey on building envelope failures in Southern British Columbia [38] showed that walls with wider overhangs had fewer moisture problems. Field measurements of WDR carried out by Ge and Krpan [39] in the same region showed that by having typical overhangs (0.3-0.6 m width) on low-rise buildings

3

and a 0.9 m overhang on a 12-story high-rise building, the deposition of WDR on the building can be significantly reduced, especially at the upper portion of the facade.

The CFD-based simulations by Blocken and Carmeliet [21] have shown that the shelter effect by roof overhang increases, for fixed wind speed and rain drop diameter, as the overhang width increases. This effect, however, decreases as wind speed increases since the trajectories become more inclined and the "sweeping effect" becomes more important. A comprehensive analysis of the effect of roof overhang on the WDR wetting of a low-rise cubic building using CFD modeling was carried out by Foroushani et al. [30]. The influence of wind speed, wind angle, and rainfall intensity was investigated for various overhang sizes. The modeling results indicated that the introduction of overhang changed both the magnitude and pattern of the WDR deposition on the façade. The impact of overhang on the WDR wetting of the façade varied locally. All the tested overhangs helped protect the upper half of the façade from WDR under all studied wind and rain conditions. The lower half of the façade, however, remained almost unaffected by the overhang. The protective effect of the overhang increases with the increase of overhang width and decrease of wind speed. Compared to rainfall intensity, both wind speed and wind angle have much greater impacts on the WDR loads and the performance of overhangs. Most recently, Kubilay et al. [32] investigated the effect of overhang and balcony projection on the WDR wetting of the façade through CFD modeling.

Although some field observations have shown that overhangs are effective in reducing WDR wetting of building facades under certain climatic conditions, there hasn't been any systematic study on quantifying the effect of overhangs on WDR loads, especially through field measurements. In many previous studies, overhangs are part of the buildings on which data is collected. The existence of the overhang is, thus, merely reported rather than being studied as a parameter. The design practice has been generally based on rule-of-thumb and governed by the architectural expression. Given the level of skepticism in the construction community on the utility of overhangs on taller buildings, and the under-appreciation of the importance of overhangs in protecting WDR in contemporary design practice, it is important that data be generated to evaluate and quantify the effect of overhang for mid-rise and high-rise buildings.

The objective of this research is to quantify the effectiveness of roof overhangs in reducing WDR loads on building façades under real life conditions through field measurements. A unique

4

adjustable overhang has been installed on a six-story building in Vancouver and two-year's wind-driven rain data has been collected and analyzed for various sizes of overhangs. This is the first time that the effect of overhang on WDR wetting of façades has been quantified through field measurements. The field data is also required to validate a CFD model, which will be used for a systematic study of various overhang designs under various climatic conditions. Ultimately, these research efforts will lead to recommendations on effective roof overhang designs for various types of buildings and climates.

2. EXPERIMENTAL SETUP

2.1 Test building

The test building is a six-story rectangular residential building with a flat roof and a short parapet located in Vancouver, British Columbia (Figure 1). The building sits atop an escarpment with the east façade facing the direction of the escarpment and is surrounded by 3-story residential buildings to its north and west and a highway to its east and south. The building is 39.2 m long, 15.2 m wide, and 19.8 m high. The building façades face the cardinal directions with one of the long façade facing the east, the prevailing wind direction. It is a fairly open site within a suburban setting, which makes it an ideal site for WDR studies.
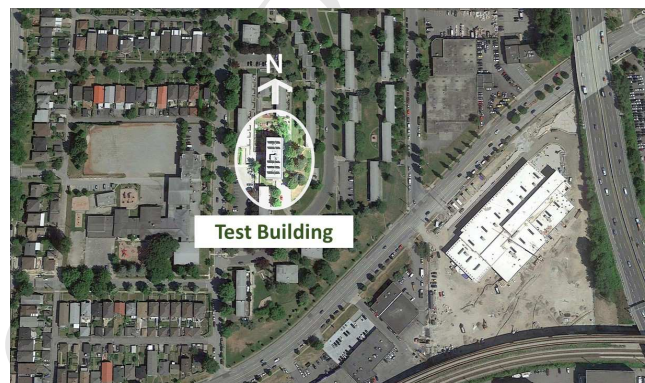

Figure 1. Aerial view of the building site (from Google Maps).

To study the effect of overhang, a customized retractable overhang structure is designed and installed on the east and north façade of the building. The retractable overhang is made up of aluminum framing structure secured to the short parapet and anodized aluminum roll shutter is attached to the frame and controlled by motor for the adjustment to represent different widths of overhang. The retractable overhang is designed as a permanent structure on the rooftop and can

withstand the wind and environmental loads as required by the building code. The retractable overhang can be changed in width ranging from 0 to 1.2 m. The overhangs are located at the northeast corner of the building covering 15 m of the east façade and 10 m of the north façade (Figure 2).
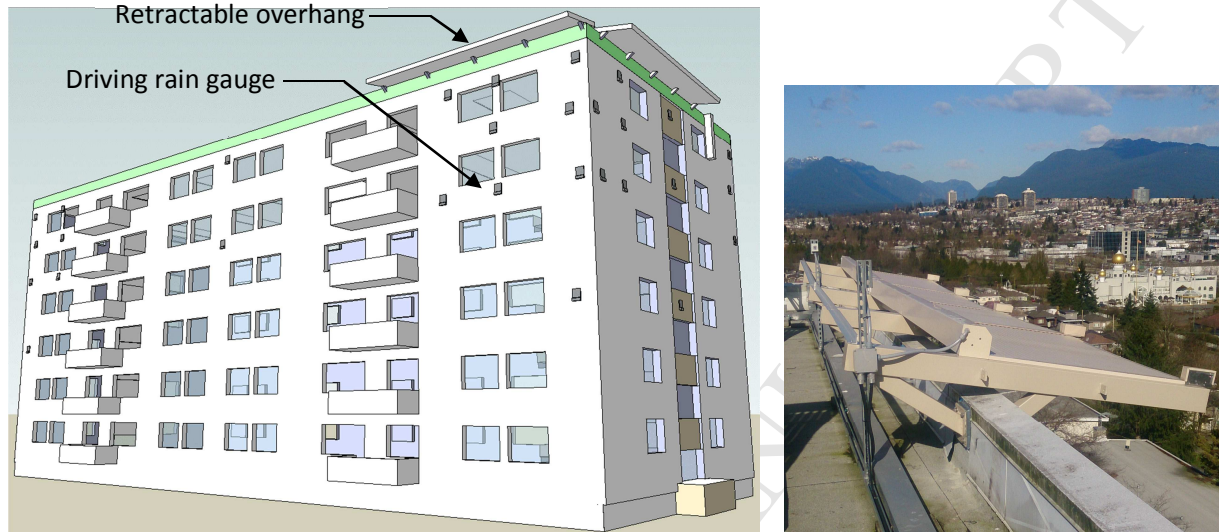

Figure 2. (a) Sketch up of the test building with the retractable overhang and wind-driven rain gauges on the east and north façades; (b) photo of installed retractable overhang (at 1.2 m).

2.2 Instrumentation

The parameters monitored include on-site weather conditions and WDR on façades. A weather station including an anemometer and a temperature and relative humidity probe is mounted on top of a tripod cross-arm that is 4.6 m above the mechanical room located on top of the main roof of the test building (Figure 3). The anemometer can measure wind speed with a range of 0–50 m/s with an accuracy of ±0.2 m/s or 1% of reading. It can measure wind direction within a range of 0–360° with an accuracy of ±0.3°. The temperature and relative humidity probe is mounted on the tripod's mast and is shielded from the sun and wind by using a radiation shield. The measurement range of the temperature sensor is -50°C to +50°C with an accuracy of ±0.1°C. The measurement range of relative humidity sensor is 0 to 100% non-condensing with an accuracy of 0.8%. The horizontal rain gauge has a conical collection area (24.5 cm diameter) constructed of gold anodized spun aluminum. The resolution of the tipping bucket is 0.1 mm/tip with an accuracy of 1% up to 50 mm/hr. The horizontal rain gauge is placed on the center of the main roof.
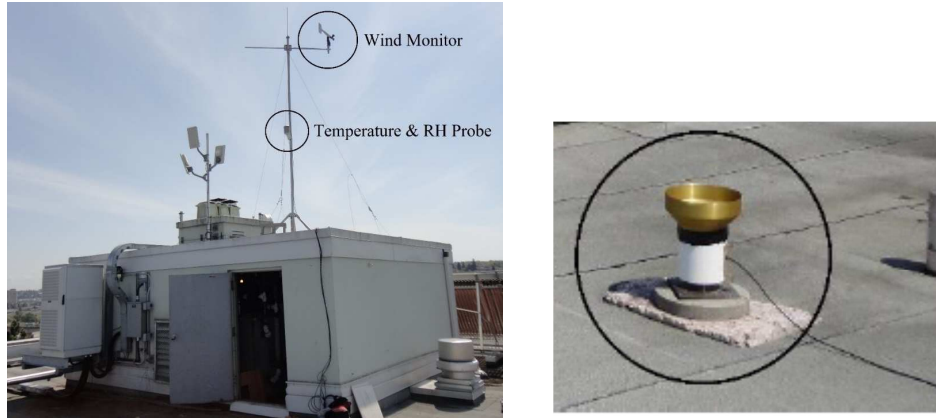
(a) weather station mast on top of the mechanical room   (b) horizontal rain gauge

Figure 3. Photo of the on-site weather station (a) wind monitor and temperature/relative humidity probe mounted on the tripod installed atop the mechanical room roof; (b) horizontal rain gauge on the main roof.

A number of customized WDR gauges are installed on the building's façades at strategically selected locations. These driving rain gauges are aluminum plate-type gauges consisting of a square collection area, 30.5 cm by 30.5 cm, i.e. 930.3 cm^2. The rain gauge is designed with details to minimize measurement errors. The choice of aluminum plate is made considering durability and good surface water runoff to reduce the adhered water. The collector's rim height is kept at 25.4 mm - a low profile to minimize wind errors. The WDR gauge has a dual tipping-bucket mechanism with a resolution of 0.06 mm/tip (Fig. 4). The tipping bucket is connected to the data logger located inside the mechanical room on the rooftop through telephone wires. A pulse signal is registered every time when the bucket is full and tipped. Figure 4 shows the details of the customized WDR gauge.
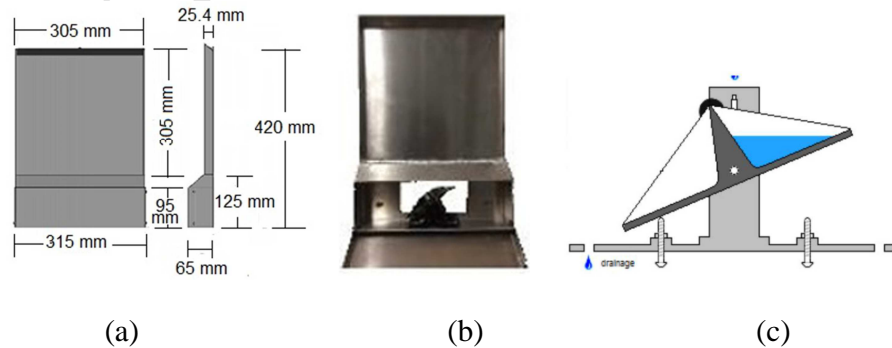
(a)   (b)   (c)

Figure 4. Customized WDR gauge: (a) profile of the WDR gauge; (b) photo; and (c) sketch of the dual tipping bucket .

The locations of WDR gauges on building façades are selected strategically based on the prevailing wind direction, building geometry and surroundings. Historical data collected from Environment Canada's National Climate Services are analyzed to identify the prevailing wind directions for the building site, which is from the east. Therefore, the majority of WDR gauges are installed on the east façade. To capture the spatial distribution of WDR on façade, the WDR gauges are placed at various locations horizontally and vertically with a focus at the top and corners to create a grid representing the typical wetting pattern on façade. Figure 5 shows the locations of on-site weather station and the exact WDR gauge locations on building facades.
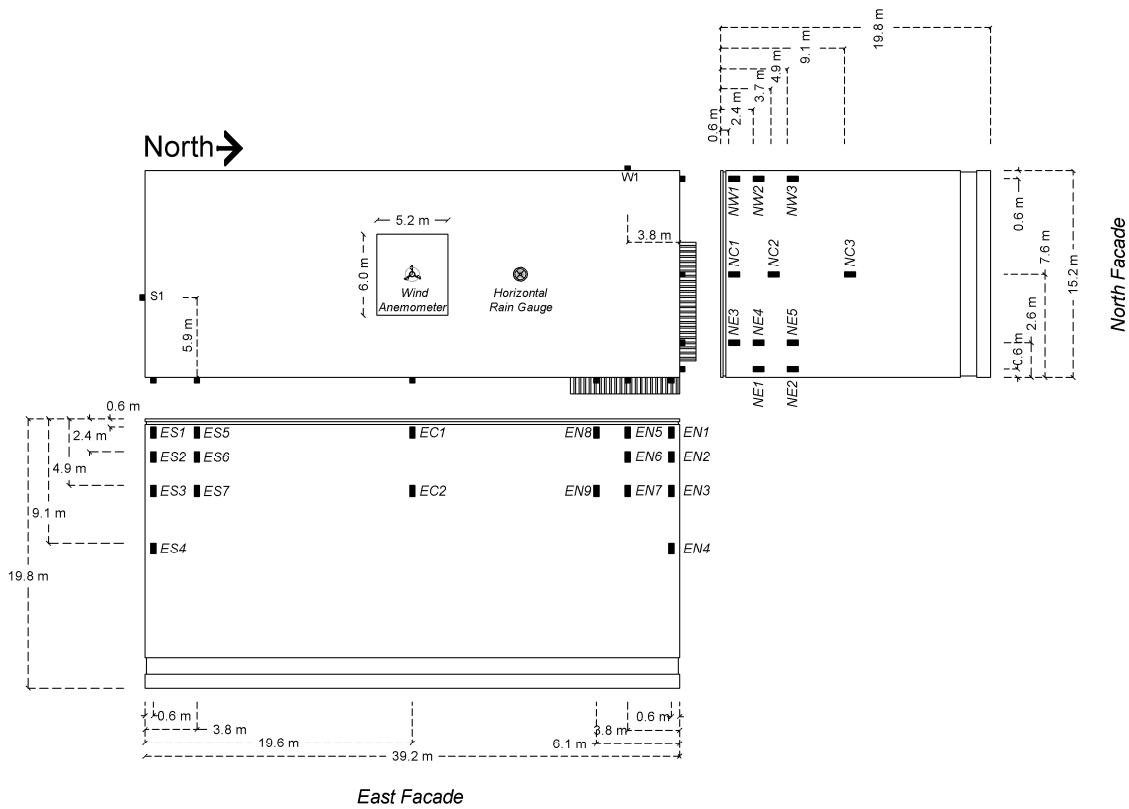

Figure 5. Location of on-site weather station and WDR gauge locations on the east and north façades.

2.3 Data collection and processing

The anemometer, temperature and relative humidity probe, horizontal rain gauge, and WDR gauges are all connected to a central data logger, which is programmed to collect and store raw

8

data every 5 minutes. The wind data (wind speed and wind direction) is gathered at 1 Hz sampling frequency and averaged every 5 minutes. The temperature and relative humidity is also averaged every 5 minutes. The sum of tips is registered for the horizontal rain gauge and the WDR gauges every 5 minutes. The data logger is connected to the internet via Ethernet, which allows the data to be collected remotely.

The data analysis reported in this paper includes: (1) on-site weather conditions (2) spatial distribution of WDR using catch ratios, and (3) effectiveness of overhang. The on-site wind data has been verified by comparison with data reported by Environment Canada from surrounding weather stations [40]. The spatial distribution of WDR on building facades is analyzed for three cases: (1) no overhang, (2) 0.6 m overhang; and (3) 1.2 m overhang. The effectiveness of the roof overhang under real-life conditions with respect to the most important meteorological parameters of wind speed and wind direction is assessed.

3. RESULTS AND DISCUSSION

3.1 On-site weather conditions

The on-site weather conditions measured from August 16, 2013 to December 2, 2015 are divided into three sub-periods: (1) no overhang, (2) with a 0.6 m overhang and (3) with a 1.2 m overhang. Figure 6 shows the wind speed, wind direction and rainfall intensity measured over the entire monitoring period.
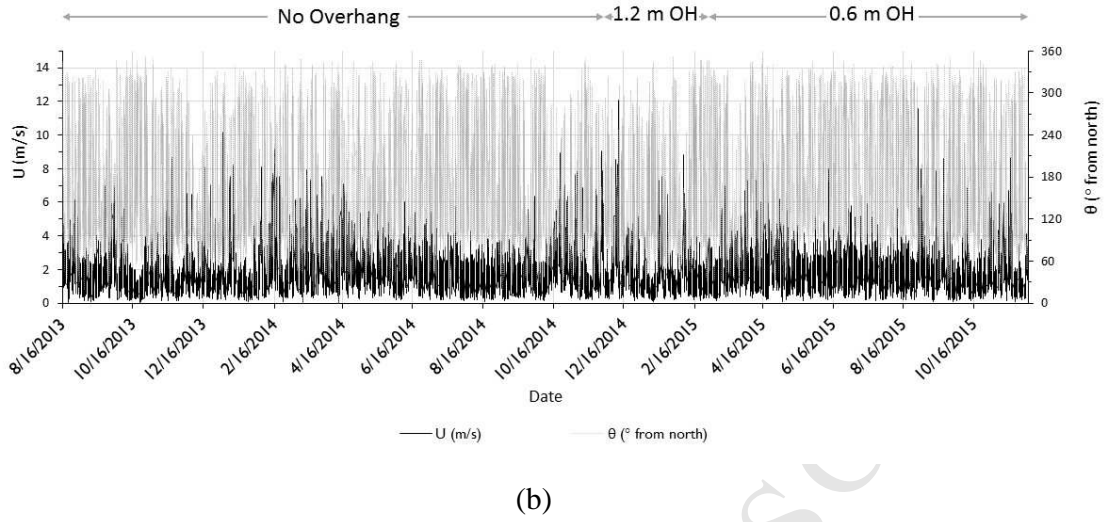

(a)

(b)
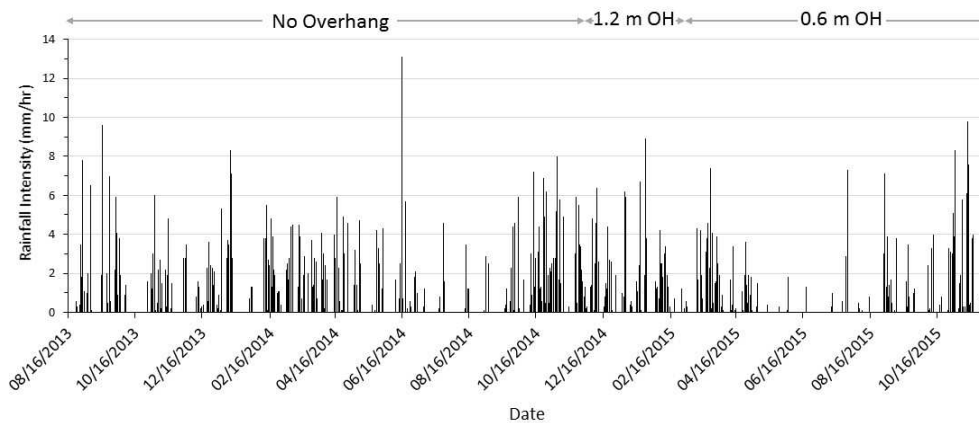
Figure 6. On-site weather data recorded over the period from Aug. 16 2013 to Dec. 2 2015: (a) rainfall intensity and (b) wind speed and wind direction.

Figure 7 and Figure 8 show the frequency distribution of wind direction and wind speed measured at the anemometer height during all hours and during rain hours for all three sub-periods, respectively. Rain hours refer to the hours during which horizontal rainfall is registered. Figure 9 shows the frequency analysis of rainfall intensity recorded over all three sub-periods. Similar wind direction and wind speed frequency distributions are observed over the three monitoring periods. The prevailing wind direction for "all hours" and "rain hours" is from the east, however, the frequency of easterly winds increases significantly during rain hours. Winds are also quite frequent from the east-south-east and east-north-east directions. This narrow band of wind directions coming from the east-north-east to east-south-east, creates an ideal opportunity to study WDR on the east facade, since the prevailing wind is blowing approximately normal to the wall. Typically, the wind speed is higher during rain hours. For "all hours", the majority of wind speeds are in the range of 0 to 2 m/s; while during "rain hours" the majority of wind speeds are in the range of 2 to 4 m/s. During "rain hours", 40 to 45% of the wind speeds are in the range of 0 to 2 m/s, 45 to 50% are in the range of 2 to 4 m/s, and less than 10% are in the range of 4 to 6 m/s. The frequency of wind speeds greater than 6 m/s is very low. The rainfall intensity is mostly light to moderate, with a rainfall intensity of less than 2 mm/hr for the majority of the time (84%), 2 to 4 mm/hr sometimes (~15%) and rarely over 4 mm/hr.

10

(a) no overhang   (b) 0.6 m overhang   (c) 1.2 m overhang

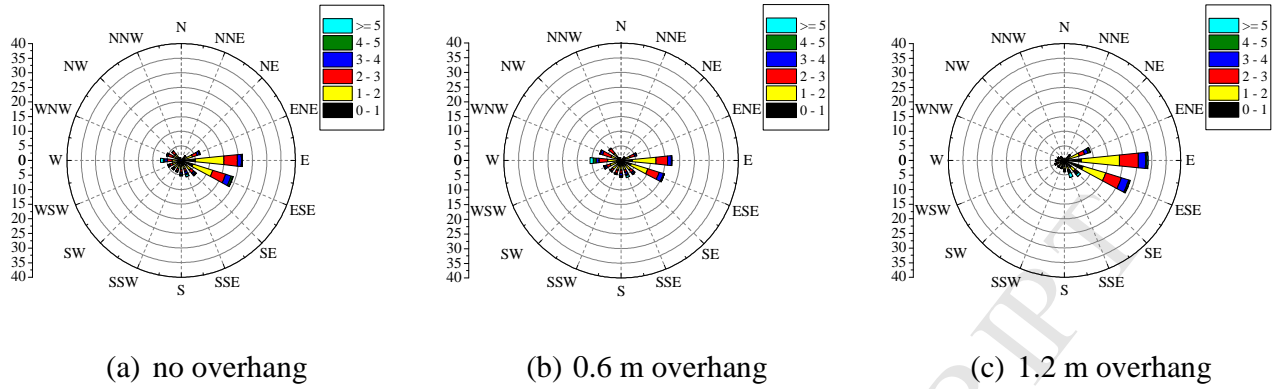Figure 7. Frequency distribution of wind direction and wind speed during all hours for all three monitoring periods.

(a) no overhang   (b) 0.6 m overhang   (c) 1.2 m overhang
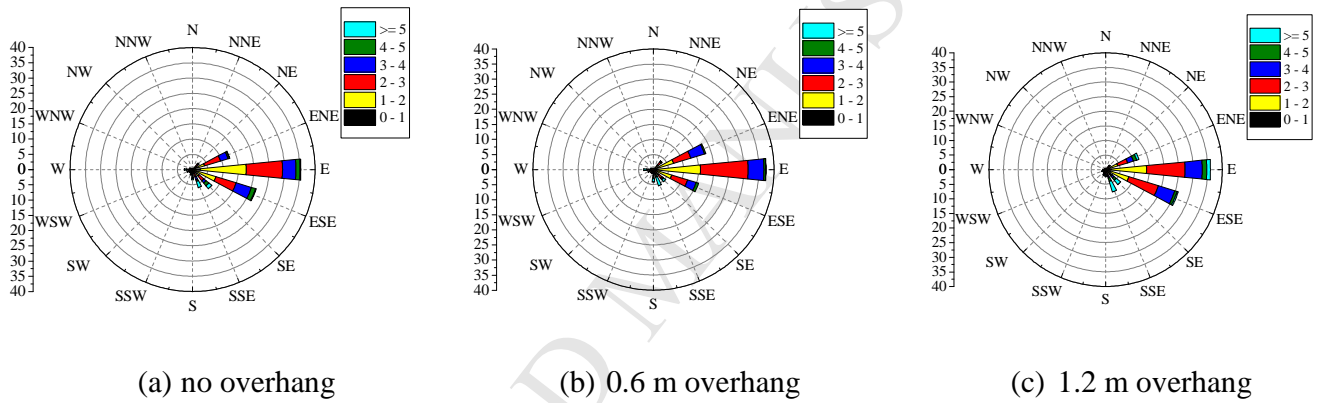
Figure 8. Frequency distribution of wind speed and wind direction during rain hours for all three monitoring periods.
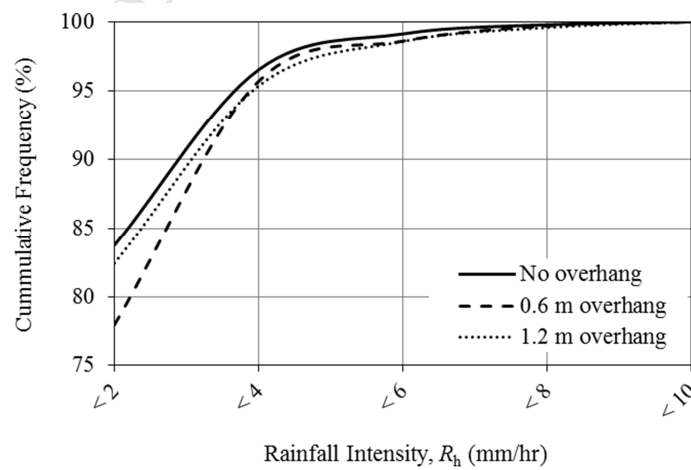

Figure 9. Cumulative frequency of rainfall intensity over the three monitoring periods.

11

On-site weather data analysis shows similar wind and rain conditions over the three monitoring periods, which allows the comparison of catch ratios on façade with and without overhang during different monitoring periods to assess the effectiveness of overhangs. This approach is referred to as similarity (repeatability), which will be discussed in section 3.3.1.

3.2 Catch ratios

The catch ratio (η) is the total amount of WDR collected on a wall surface (S_{wdr}) divided by the total amount of horizontal rainfall (S_h) over the same time period:

$$\eta = \frac{S_{wdr}}{S_h} \tag{1}$$

Catch ratios are calculated for each monitoring period to show the spatial distribution of WDR across the building facades. The catch ratios are then used to evaluate the effectiveness of overhang.

3.2.1 Error analysis of WDR measurements

There are mainly five types of possible error sources in WDR measurements [13]: (1) evaporation of adhesion water from the collection area; (2) evaporative losses from the reservoir, i.e. tipping bucket; (3) splashing of drops from the collection area; (4) condensation on the collection area; and (5) wind errors due to the disturbance of wind-flow pattern and raindrop trajectory by the gauge body. Evaporation loss from the reservoir, the tipping buckets, in our study, is negligible given that the tipping buckets with a small volume of 5.5g are enclosed and the relative humidity is typically high, over 90% RH during rain. Splashing of raindrops mainly occurs during heavy rainfalls with high wind speed and large raindrops. Therefore, splashing errors are considered to be negligible given the low wind speed and the low horizontal rainfall intensity values as shown in Figures 8 and 9. The undercooling condensation on the WDR gauge during a rain event is also typically negligible since the overcast sky limits radiation loss [13, 18]. Wind errors caused by the presence of rain gauge itself are minimized by the customized WDR gauge design with a low rim height of 25.4 mm. In addition, the wind speed close to the wall surface is low.

During and after the rain, some rainwater is adhered to the collection area of the gauge, which is not collected by the tipping bucket and remains unmeasured. With time, this adhesion water

evaporates. The error associated with the evaporation of adhesion water from the gauge catch area (or collection area) is the largest and can be as high as 100% [13]. There is an additional error when using tipping bucket mechanism for WDR measurement, which is rest water error, E_{RW}. A tip is registered only when the tipping bucket is completely filled. The water remained in the tipping bucket at the end of a rain spell is not registered for this spell. If the water does not evaporate before the start of the next spell, it will be added to the new spell. The rest water error can occur during every hour, however, when considering the total amount of WDR for one entire rain event, it only occurs once at the end of the rain event since positive and negative errors from one hour to the next balance out during the rain event [22]. The water in the tipping bucket that remains after each tip can be as large as the maximum amount the tipping bucket can hold. At the end of each rain event, it is assumed that one tipping bucket's amount of water is lost due to evaporation during dry periods before the next rain event starts. Therefore, only adhesion-water-evaporation and rest water errors are considered in the error analysis.

It is assumed that all the adhered water will evaporate during the dry periods i.e. the hours without any WDR collected within the rain event. Therefore, the number of interruptions (i.e. hours without WDR collected) is counted within each rain event. Laboratory tests found the adhesion-water to be an average of approximately 4.7 g on the collection area, which is equal to 0.050 mm for a collection area of 930.3 cm^2 of the customized WDR gauges used in this study. Thus, the total amount of adhesion-water-evaporation is the number of interruptions multiplied by 0.05 mm. To account for the rest water error, the amount of water held by the tipping bucket is counted once for each rain event. The tipping bucket can hold 5.5g or 0.060 mm/tip with a collection area of 930.3 cm^2.

The total error associated with WDR measurements using the customized WDR gauge is calculated as follows:

$$e_{TOT} = \frac{E_{TOT}}{S_{WDR}} \tag{2}$$

$$E_{TOT} = E_{AW} + E_{RW} \tag{3}$$

where,

E_{AW}=Number of interruptions x 0.05mm;

13

E_{RW}=the amount of water held by the tipping bucket for 1 tip, 5.5 grams, which is equivalent to 0.06mm for a collection area of 930.3cm^2

$$S_{WDR} = n \times V_{BOWL}$$

n=number of tipping bucket tips registered for each rain event;

V_{BOWL}=the amount of water the tipping bucket can hold, 5.5 grams, which is equivalent to 0.06 mm for a collection area of 930.3cm^2

Eq. (2) becomes

$$e_{TOT} = \frac{E_{AW}}{n \times 0.06} + \frac{1}{n}$$

(4)

Equation 4 is used to estimate the total error that may occur for WDR measurements during each rain event. Rain events are identified according to the ISO standard ISO 15927-3 [41], which defines a rain event as having at least 96 hours' dry period between two rain events.

The total error decreases exponentially with the increase of WDR. For smaller amounts of WDR, (i.e. light rainfall event or at locations that receive smaller amounts of WDR), the error could be as high as 100%, as shown in Figure 10. As an example, Table 1 shows the error estimates for the WDR measurements on the WDR gauges installed on the south corner of the east façade during a rain event from February 10 to February 25, 2014. The total amount of rainfall for the rain event is 162.8 mm with an average rainfall intensity of 1.1 mm/hr. For this particular rain event, the measurement errors range from 2.7-9.2% and decrease with the increase of WDR amount measured. The measurement errors are taken into account for the WDR analysis in this paper.
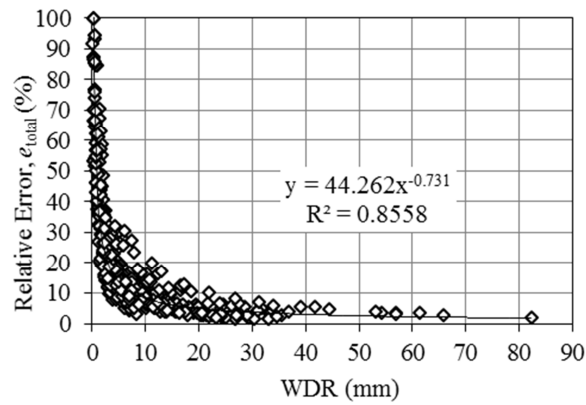
Figure 10. Errors in relation to WDR amount.

Table 1. Error estimates for WDR measurements on south corner of the east façade during the rain event from February 10 to February 25, 2014 (total WDR amount of 162.8 mm, wind speed of 2.4 m/s and wind direction of east and east-south-east)

WDR gauge	ES1	ES2	ES4	ES5	ES6	ES7
No. of Tips	750	419	164	547	369	268
No. of Interruptions	23	23	17	26	21	16
S_{wdr} (mm)	45.00	25.14	9.84	32.82	22.14	16.08
E_{AW} (mm)	1.15	1.15	0.85	1.3	1.05	0.8
E_{RW} (mm)	0.06	0.06	0.06	0.06	0.06	0.06
E_{TOT} (mm)	1.210	1.210	0.910	1.360	1.110	0.860
e_{TOT} (%)	2.7	4.8	9.2	4.1	5.0	5.3

3.2.2. Catch ratio on east façade

Figure 11 shows the catch ratio contours generated based on the point measurements on the east façade for the three monitoring periods. The measured values are also shown in Figure 11. The catch ratio contours on the east façade were generated using the catch ratios measured at the eighteen WDR gauges installed on the façade. The Kriging gridding method in Surfer 11 was used for the contour generation as Kriging method gave the best mapping for the given dataset. The Kriging method is best used for spatial analysis and is a method of interpolation for which the interpolated values are modeled by a Gaussian process governed by prior co-variances. The amount of rain deposited on the building facade varies with locations, however, a symmetrical distribution of WDR across the east facade can be observed during the period without overhang given that the prevailing wind direction is from the east most of the time resulting in the wind blowing normal to the façade. The classic wetting pattern can be observed: (1) the top corners are

15

the most wetted followed by the top and side edges and (2) wetting increases from the bottom of the facade to the top and from the middle of the facade to the sides. With overhangs added (Figure 11b and Figure 11c), the majority of the catch ratios on the east facade are similar to that of the monitoring period without overhang (Figure 11a) since both prevailing wind directions are from the east with similar wind speeds and horizontal rainfall intensities. However, it is evident that the gauges below the overhang have lower catch ratios when compared to: (1) other gauges of similar height and distance from edge and (2) the same gauges during the monitoring period without overhang (Figure 11a). The gauges right below the overhang are the most protected (EN1, EN5, EN8). The protection provided by the 0.6 m overhang seems to extend to 2.4 m to 4.9 m (second to third row of WDR gauges), and the protection provided by the 1.2 m overhang seems to extend to 4.9 m to 9.1 m (third to fourth row of WDR gauges) when compared to the period without overhang. The overhang is less effective in reducing WDR deposition near the edge of the wall. The protection increases from the side edge to the center of the facade and from the bottom to the top of the facade.
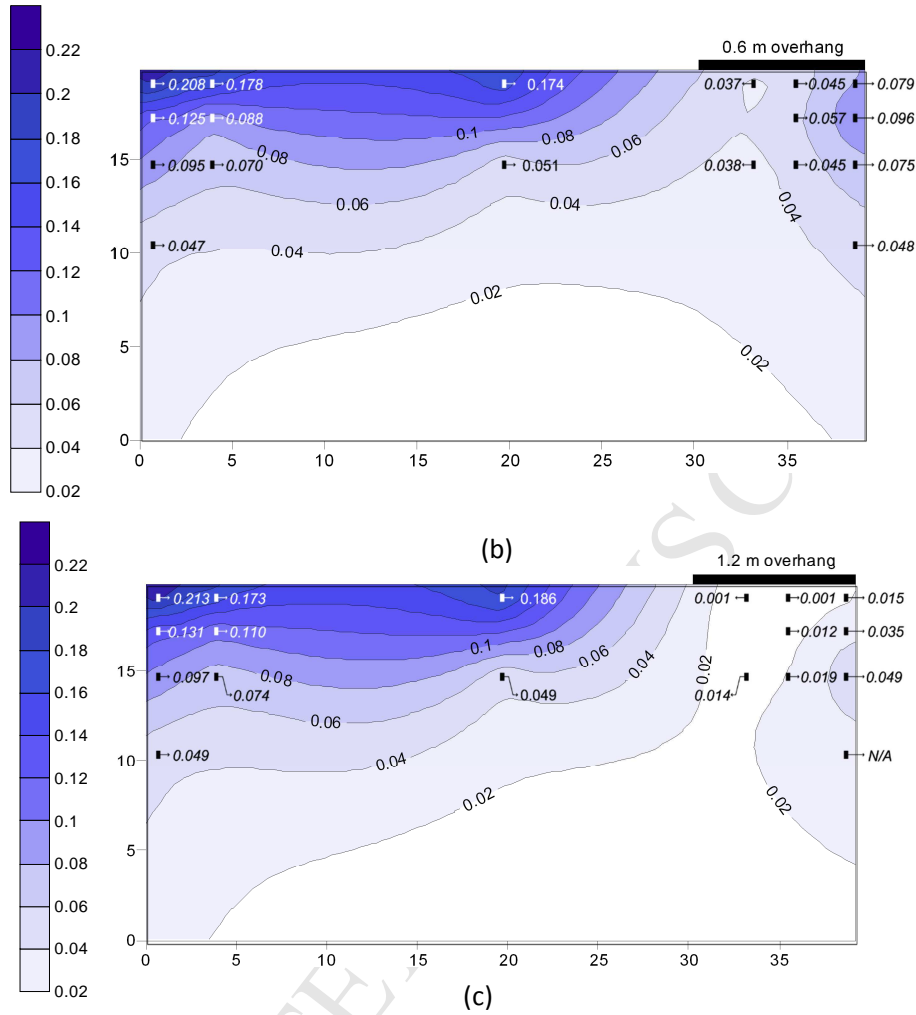

(a)

16
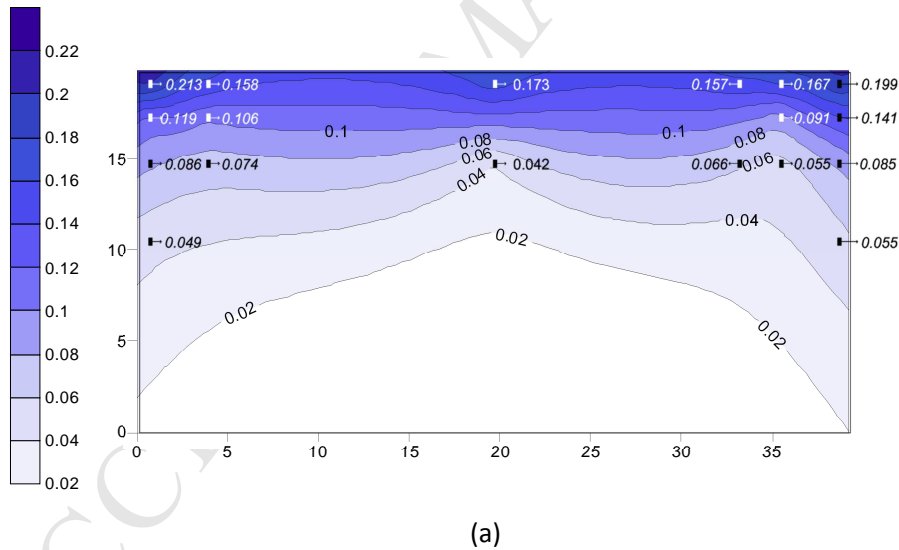
Figure 11. Catch ratios on the east façade: (a) no overhang; (b) 0.6 m overhang and (c) 1.2 m overhang. Note: contours are generated based on measurements. Measured values are shown besides the rectangular box representing the WDR gauge.

Since the prevailing wind direction is from the east, the catch ratios on the north facade are not symmetrical and are much lower than that on the east façade (Figure 12). The gauges on the left edge of the facade (NE1 and NE2) receive less rain than the gauges located to their right. This may be explained by considering the wind flow around the building. Since the prevailing wind direction during rain hours is from the east, flow separation occurs at the edges of the east facade, resulting in a wetting pattern that is reflective of the wind flow around the north-east edge.

3.2.3. Catch ratio on north façade

The catch ratios on the north facade at locations not-affected by the overhang are slightly higher for the monitoring period with a 0.6 m overhang when compared to the monitoring period

without overhang. This is due to an increase in frequency of north-easterly winds for the monitoring period with a 0.6 m overhang. The locations right below the 0.6 m overhang (NE3 and NC1) are the most protected having significantly lower catch ratios when compared to NW1, which is at the same height. This is also apparent when compared to the north facade without overhang (Figure 11a). The remaining locations below the 0.6 m overhang are protected to various degrees. With a 1.2 m overhang, the catch ratios on the north facade at locations not affected by the overhang are similar to the catch ratios for the period without overhang because of the similar on-site weather conditions. The locations right below the overhang (NE3 to NC1) are entirely protected. The remaining locations below the overhang are protected to various degrees and seem to extend up to half of the building height (i.e. the fourth row of gauges).

(a) (b) (c)
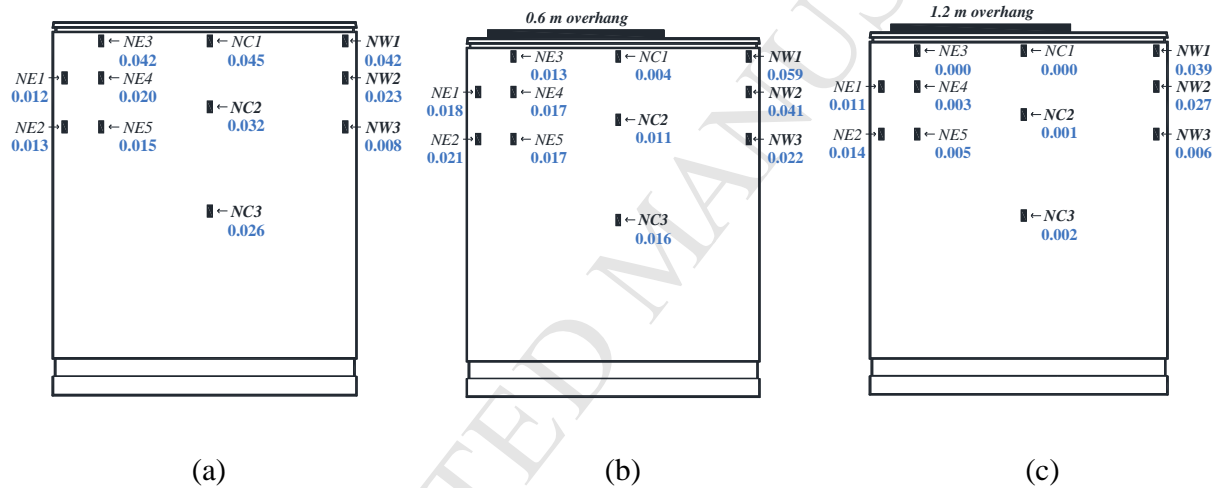
Figure 12. Catch ratios on the North façade: (a) no overhang (b) 0.6 m overhange and (c) 1.2 m overhang.

3.3 Effectiveness of overhang

The effectiveness of overhang, δ, is defined as the percentage reduction in catch ratios with and without the overhang. The overhang effectiveness is assessed by two approaches: 1) similarity, which compares two similar rain events during the periods with and without overhang; and 2) symmetry, which uses a symmetrical distribution of WDR across the building facade during a rain event. The effectiveness of overhang with respect to wind speed and wind incident angles is analyzed.

$$\delta = \frac{\eta - \eta_{OH}}{\eta} \times 100 \qquad (5)$$

18

where η is the catch ratio without overhang, $η_{OH}$ is the catch ratio with overhang.

3.3.1 Similarity

The overhang effectiveness can be assessed by comparing the catch ratios at the gauge locations that are directly under the overhang (gauges EN1 to EN9) in one rain event with the catch ratios at the same gauge locations in a similar rain event without overhang. To establish similarity, both rain events should have similar meteorological characteristics, i.e. wind speed, wind direction and rainfall intensity, ultimately leading to similar catch ratios at the gauge locations that are not influenced by the overhang. Once this similarity has been established, the catch ratios at gauge locations EN1 to EN9 (under the overhang) during rain events without overhang can be compared to the catch ratios during rain events with overhang. As an example, Figure 13 shows the wind and rain conditions of two similar rain events (RE), i.e. (RE) 7 during the period without overhang, and (RE) 16 during the period with the 1.2 m overhang.

Rain event 7 started on February 10 and ended on February 25, 2014. It is characterized by a light to moderate rainfall intensity with less than 2 mm/hr the majority of the time (80%), 2-4 mm/hr occasionally (18%), and rarely reaching above 4 mm/hr (2%). The total horizontal rainfall amount of this rain event is 162.8 mm. The wind speed during rain hours is mostly in the range of 0-4 m/s (86%) and occasionally above 4 m/s (14%). The wind direction during rain hours is predominantly from the east followed by the east-south-east. Rain event 16 began on December 4, 2014 and ended on December 11, 2014. In comparison to rain event 7, the rainfall intensity is similar with a rainfall intensity under 2 mm/hr the majority of the time (74%), 2-4 mm/hr occasionally (21%) and rarely reaching above 4 mm/hr (4%). The total horizontal rainfall amount of this rain event is 132 mm. The wind speed during rain hours is mostly in the range of 0-4 m/s (74%) and occasionally above 4 m/s (26%). The wind direction during rain hours is predominantly from the east-south-east followed by the east.

19
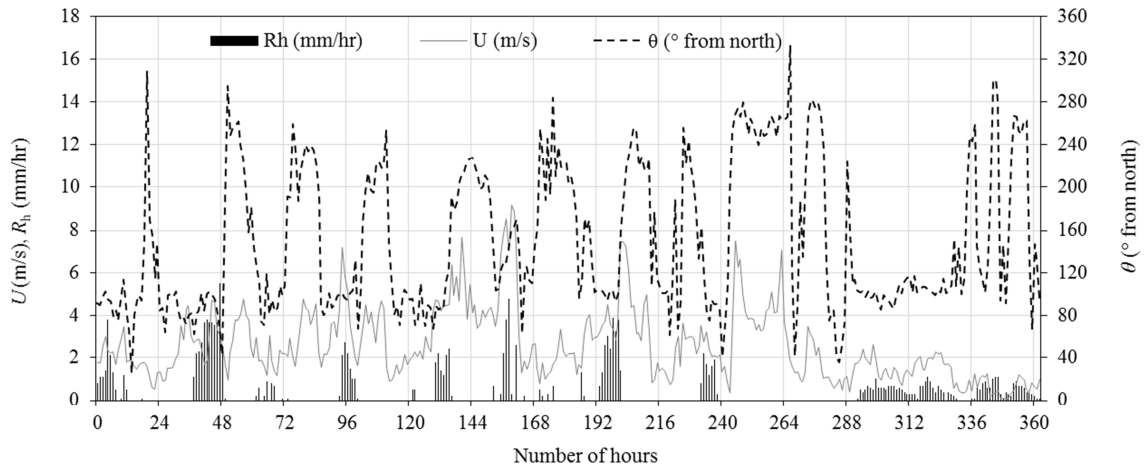
(a) Rain event 7: no overhang (February 10 to February 25, 2014).

Total rainfall=162.8mm, no. of rain hours=145hrs, average wind speed= 2.36 m/s, Average arithmetic wind direction 124°, average rainfall intensity=1.1mm/hr.
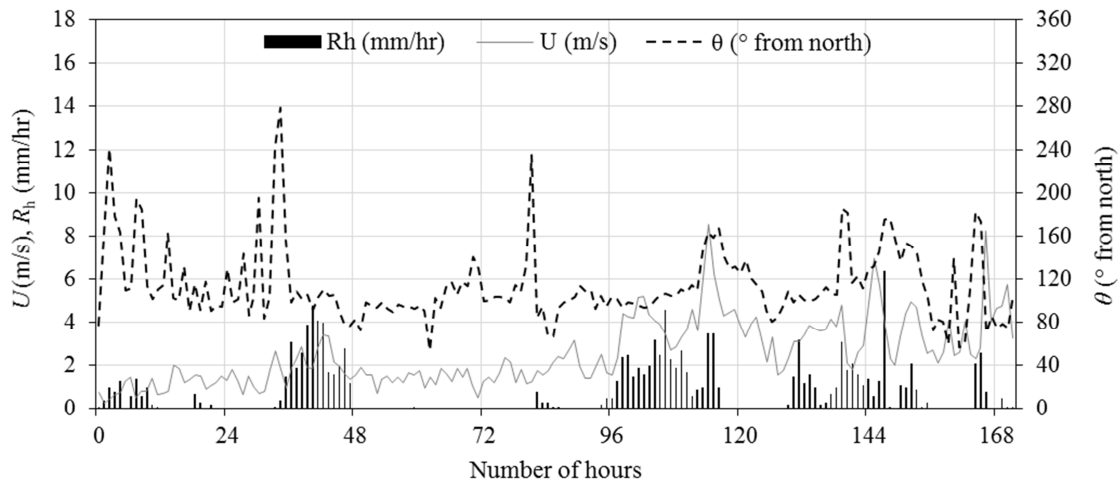
(b) Rain event 16: 1.2m overhang (December 4 to December 11, 2014).

Total rainfall=132mm, no. of rain hours=90hrs, average wind speed=3.05 m/s, Average arithmetic wind direction 121°, average rainfall intensity=1.5mm/hr.

Figure 13– Rainfall intensity (R_h), wind speed (U), and wind direction (θ) for two rain events: (a) rain event 7: no overhang and (b) rain event 16: 1.2 m overhang.

The catch ratios for rain events 7 and 16 are shown in Table 2. The similar meteorological parameters between these two rain events yield similar catch ratios on the gauges not sheltered by the overhang, which are the un-shaded values (EC1, EC2, ES1 to ES7). Catch ratios are

slightly higher for rain event 7, probably due to slightly higher frequency of wind coming from east-south-east. The difference of catch ratios at these locations is typically within 10%. The effectiveness of overhang, i.e. percentage of reduction, is calculated using catch ratios for rain event 7 as the references for gauge locations underneath the retractable overhang, which are shaded (EN1 to EN9).

Table 2. Catch ratios and overhang effectiveness on the east façade for rain events 7 and 16.

WDR Gauge	Catch Ratios		Overhang Effectiveness (%)
	RE 7 (No OH)	RE 16 (1.2 m OH)	
EN1	0.281	0.019	93
EN2	0.169	0.051	70
EN3	0.118	0.056	52
EN4	0.074	n/a*	
EN5	0.228	0.005	98
EN6	0.121	0.024	80
EN7	0.070	0.026	63
EN8	0.210	0.003	98
EN9	0.073	0.017	76
EC1	0.217	0.202	
EC2	0.050	0.057	
ES1	0.284	0.266	
ES2	0.162	0.168	
ES3	n/a	0.117	
ES4	0.066	0.059	
ES5	0.210	0.186	
ES6	0.143	0.132	
ES7	0.104	0.091	

Shaded rows catch ratios for WDR gauges located under the retractable overhang. Data for gauge EN4 was not available during this period due to hardware malfunction.

A number of similar rain events are identified for 0.6 m overhang and 1.2 m overhang. The percentage reduction in catch ratios, i.e. overhang effectiveness, is calculated for each pair of rain

events. Given that the WDR deposition on façade is highly dependent on the meteorological parameters and that the catch ratios vary over different rain events, each comparison yields a different percent reduction in catch ratio for the same gauge location and an average is used to report the effectiveness of overhangs. Table 3 lists the overhang average effectiveness with the standard deviation.

Table 3. Overhang effectiveness on the east façade (in %)

WDR Gauge	0.6 m		1.2 m	
	Average	Standard deviation	Average	Standard deviation
EN1	75	9	93	6
EN2	54	8	77	12
EN3	36	18	48	21
EN4	33	15	n/a*	
EN5	88	5	99	1
EN6	55	11	88	7
EN7	42	11	69	13
EN8	86	6	99	1
EN9	57	14	81	8

*Note: *Data for gauge EN4 was not available during this period due to hardware malfunction.*

3.3.2 Symmetry

As shown in Figure 11a, the catch ratios are more or less symmetrical on the east façade given that the predominant wind direction is from the east during rain hours, which is normal to the façade. Therefore, a symmetrical distribution of WDR can be assumed to evaluate the effectiveness of overhang by directly comparing the catch ratios at gauge locations underneath the overhang on the north side of the façade (EN1 to EN7) to those on the south side of the façade (ES1 to ES7), which do not have an overhang above them. Rain events with the prevailing wind direction coming from the east are selected and the percentage reduction in catch ratios for a 0.6 m overhang and 1.2 m overhang are calculated. The meteorological parameters between rain events differ from one another resulting in different percent reductions in catch ratio for the

same gauge location, the average is used to report the effectiveness of overhangs. Table 4 lists the average overhang effectiveness with the standard deviation.

Table 4. Overhang effectiveness on the east façade (in %)

WDR Gauge	0.6 m		1.2 m	
	Average	Standard deviation	Average	Standard deviation
EN1 vs ES1	69	14	93	4
EN2 vs ES2	37	12	74	12
EN3 vs ES3	23	17	49	17
EN4 vs ES4	36	16	n/a*	
EN5 vs ES5	85	9	99	1
EN6 vs ES6	47	8	89	6
EN7 vs ES7	40	18	74	9

*Note: *Data for gauge EN4 was not available during this period due to hardware malfunction.*

3.3.3 Discussion: Similarity vs Symmetry

The average percentage reductions in catch ratio calculated for gauge locations on the east façade using both methods are compared (Figure 14). In general, there is a good agreement between these two methods with a difference between 0 to 35%.

For the 0.6 m overhang, the average percent reductions calculated using the similarity approach are slightly higher than those calculated using the symmetry approach. The highest discrepancy is for gauge EN3 (35%) followed by EN2 (31%) and EN6 (14%). For other gauges, the discrepancy is below 10%. For the 1.2 m overhang, the average percent reductions in catch ratios are almost identical for both methods (0-7% difference). As expected, larger overhang provides better protection. The effectiveness of 1.2 m overhang ranges from 50% to 99%, while the effectiveness of 0.6 m overhang ranges from 40% to 85%.
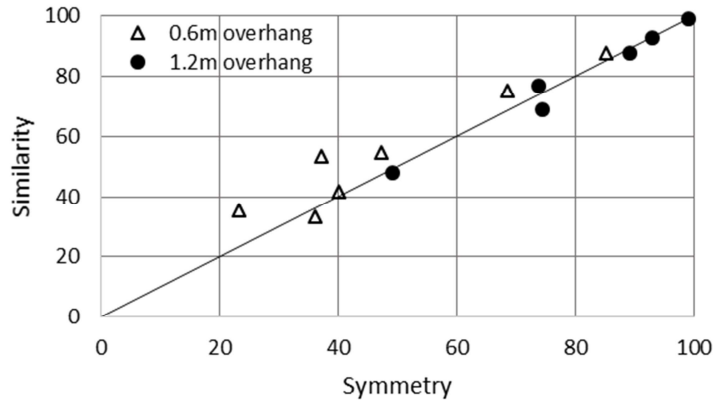
Figure 14. Comparison of overhang effectiveness calculated using similarity and symmetry approaches for gauges on the east façade.

3.3.4 *Quantification of overhang efficiency*

Given the similar results obtained by similarity and symmetry approaches and the predominantly easterly winds do not allow for symmetry analysis on the north facade, the effectiveness of overhang calculated using the similarity approach is used in the following sections for discussion purposes. The effectiveness of overhangs is shown in Figure 15 for the east façade and in Figure 16 for the north façade, respectively.
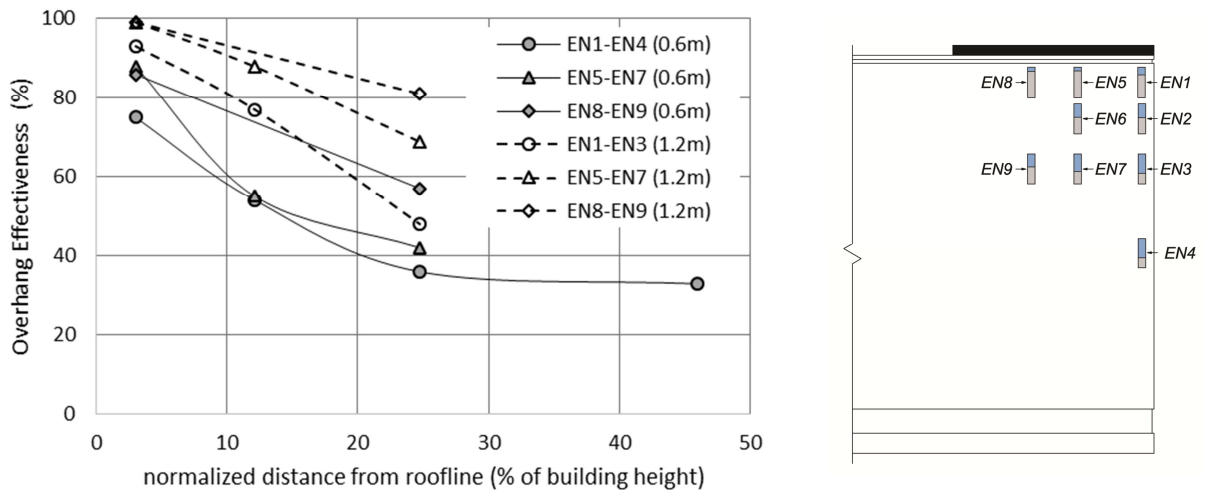

Figure 15. Effectiveness of overhangs on the east façade.

For the east façade, the effectiveness of the overhang decreases when moving from the upper edge towards the ground and from the center towards the side edge of the façade. The overhang

reduces the WDR deposited on the façade, especially the area right beneath the overhang (EN1, EN5, EN8 at 0.6 m below the roofline, i.e. 3% of the building height). For a 0.6 m overhang the reduction is about 75 to 90% and for a 1.2 m overhang the reduction is greater than 90%. At a distance of 2.4 m below the roofline (i.e. 12% of the building height, EN2 and EN6), the WDR reduction is 50% for the 0.6 m overhang and 80-90% for the 1.2 m overhang, respectively. At a distance of 4.9 m below the roofline (i.e. ¼ of the building height, EN3, EN7, EN9), the WDR reduction is about 36 to 60% for the 0.6 m overhang and 50-80% for the 1.2 m overhang, respectively. The protection area can extend up to 9.1 m below the roofline (i.e. about 45% of the building height, EN4) with the similar amount of WDR reduction as at a distance of 4.9 m below the roofline for the 0.6 m overhang. Due to the malfunction of EN4 gauge, data is not available for 1.2 m overhang, however, it is expected that the 1.2 m overhang would provide at least similar if not better performance than the 0.6 m overhang. The level of protection is dependent on the wind and rain conditions.

A similar trend is observed for the north façade. In general, as expected a larger overhang provides better protection, particularly at locations close to the center and the top of the facade. At mid-height of the building (9.1 m below the roofline), an 83% reduction in WDR can be provided by the 1.2 m overhang at the centre of the façade. A slightly greater protection is observed for north façade at the same building height probably due to the wind being oblique to the façade most of the time. The influence of wind speed and wind direction on the effectiveness of overhang is discussed in the following section.
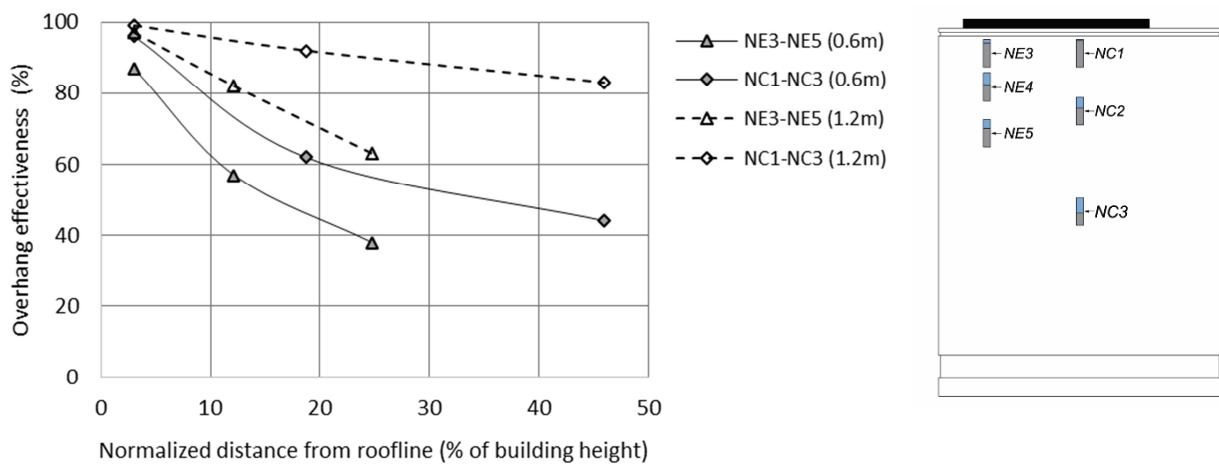

Figure 16. Effectiveness of overhangs on the north façade.

25

To quantify the effect of overhang on the reduction of WDR impinged on the façade, an area-weighted average catch ratio ($\overline{\eta}$) is introduced (equation 6) to calculate the area-weighted overhang effectiveness for four areas shown in Figure 17, namely A1, A2, A3 and A4 representing 15%, 30%, 60% and 100% of the façade area, respectively. This evaluation is carried out for the case with overhang covering only the north side of the east façade, as tested, (i.e. partial overhang) first followed by the case assuming that the entire façade width is fitted with overhang (i.e. full overhang) to generalize the results. For the case with partial overhang, the area-weighted catch ratios calculated for façade area underneath the overhang on the north side are compared to those calculated for the same façade area on the south side. For the case with full overhang assumed, the area-weighted catch ratios calculated based on measurements with overhang are compared to those calculated based on measurements without overhang. The detailed calculation procedure is explained as follows.
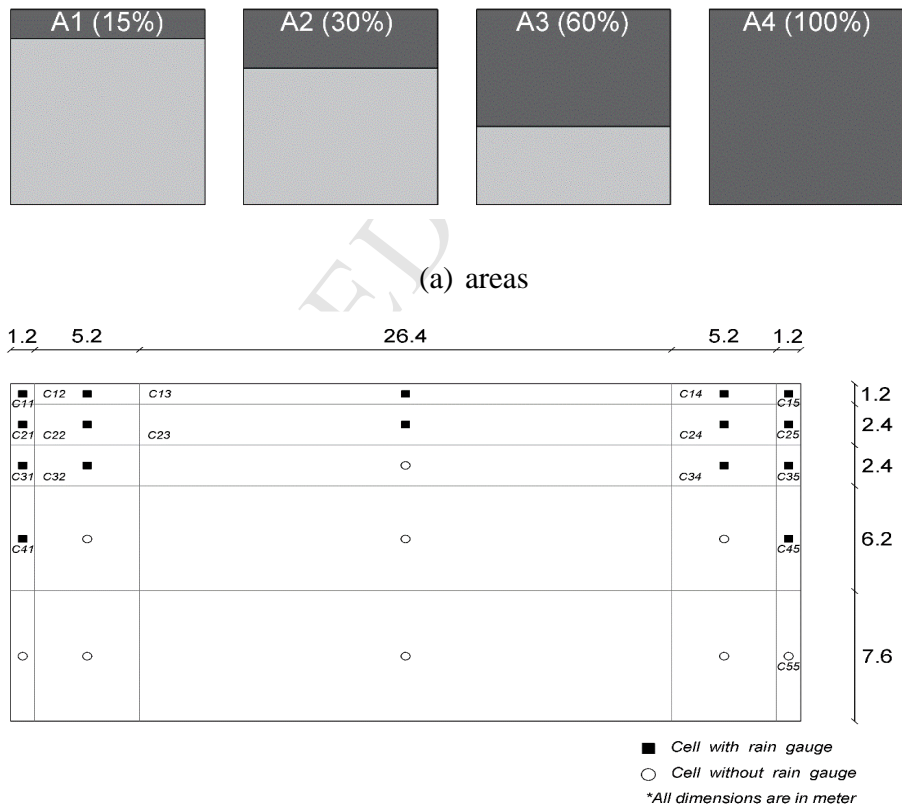

(a) areas

(b) cells

Fig. 17. Areas (a) and cells (b) on the east façade for the calculation of area-weighted overhang effectiveness.

26

$$\bar{\eta} = \frac{1}{\sum_{i=1}^{n} A_i} \sum_{i=1}^{n} \eta_i A_i \tag{6}$$

where, the summation index i is the cell number, A_i is the area of the ith cell and n is the total number of the cells over which the average is calculated. The façade is divided into cells in such a way that rain gauges are located in the centre of a cell. There are in total eighteen rain gauges installed on the east façade (Fig. 5). The catch ratios at the 3rd column rain gauges (EN8 and EN9) are similar to the catch ratios measured at the 2nd column rain gauges at the same height (EN5 and EN7) as shown in Fig. 11a. The 3rd column rain gauge locations are within the cell defined by the 2nd column rain gauge, which confirms the assumption of a constant catch ratio within the cell being reasonable. In addition, the 3rd column rain gauges are only installed on the north side of the east façade. Therefore, sixteen rain gauges except for EN8 and EN9 are used to define the cells for calculating the area-weighted average overhang effectiveness, which result in twenty-five cells, five columns and five rows on the east façade (Fig. 17b). For the cells with rain gauge, a constant catch ratio is assigned with value measured by the gauge located in its centre. For the remaining nine cells that located at the lower and centre parts of the façade, a constant catch ratio interpolated from the adjacent cells is assigned using the catch ratio contours generated (Fig. 11). For these areas, the catch ratios are quite small.

For the partial overhang case, the first two columns of cells are used for the calculation. As discussed in section 3.3.3, the WDR distribution on the east façade is more or less symmetrical, therefore, the area-weighted catch ratios calculated for the area underneath the overhang on the north side is compared to those calculated for the area without overhang on the south side.

For the full overhang case, the catch ratio of each cell is determined for the case without overhang first. Given the symmetrical WDR distribution on the east façade, an average of the measured catch ratios at two symmetrical locations is assigned to both cells located symmetrically on the façade. For example, the average of catch ratios measured at gauges EN1 and ES1 without overhang is assigned to both C_{11} and C_{15}. When the overhang is fitted, the same catch ratio measured underneath the overhang is assigned to the cell located symmetrically on the south side. For example, catch ratios measured at gauge EN1 with overhangs are assigned to both C_{11} and C_{15}. In the field measurements, rain gauges located at the center of the façade (EC1 and EC2) are not covered by the overhang, therefore, no overhang effectiveness available for these

centre locations. The overhang effectiveness determined for 2nd column rain gauges is applied to these centre locations, which is a conservative assumption given that the effectiveness increases when moving from the side edge towards the centre of the façade, as shown in Fig. 15 and Fig. 16. The results are listed in Table 5 for the partial overhang case and in Table 6 for the full overhang case, respectively.

Table 5. Effect of overhang on WDR reduction on the east façade (partial overhang)

Façade area	No overhang (south side)		0.6 m overhang (north side)		1.2 m overhang (north side)	
	$\sum_{i=1}^{n} \eta_i A_i$	WDR distribution on façade (%)	$\sum_{i=1}^{n} \eta_i A_i$	Area-weighted effectiveness (%)	$\sum_{i=1}^{n} \eta_i A_i$	Area-weighted effectiveness (%)
A1 (15%)	4.6	42.9	1.4	68.6	0.4	91.4
A2 (30%)	6.4	60.0	2.5	60.9	1.0	84.3
A3 (60%)	8.9	84.0	4.2	52.9	2.4	73.6
A4 (100%)	10.7	100	5.9	44.8	4.1	61.8
Total WDR reduction (%)			44.8		61.8	

Table 6. Effect of overhang on WDR reduction on the east façade (full overhang)

Façade area	No overhang		0.6 m overhang		1.2 m overhang	
	$\sum_{i=1}^{n} \eta_i A_i$	WDR distribution on façade (%)	$\sum_{i=1}^{n} \eta_i A_i$	Area-weighted effectiveness (%)	$\sum_{i=1}^{n} \eta_i A_i$	Area-weighted effectiveness (%)
A1 (15%)	18.2	53.0	5.5	70.0	1.4	92.2
A2 (30%)	23.2	67.6	8.4	63.7	3.1	86.8
A3 (60%)	29.9	87.4	12.9	56.8	6.7	77.7
A4 (100%)	34.3	100	17.3	49.6	11.0	68.0
Total WDR reduction (%)			49.6		68.0	

The results for the case with partial overhang are close to those found for the case with full overhang but slightly lower as expected since the overhang covers 25% of the façade width from the edge and the overhang effectiveness increases while moving towards the centre of the façade.

As shown in Table 6, without overhang, the top 15% of the façade area receives 53% of the total WDR impinged on the entire façade. The total amount of WDR impinged on the façade can be reduced by 50% with a 0.6 m overhang and by 68% with a 1.2 m overhang, respectively. For both overhangs, 70% of the total WDR reduction is attributed to the top 15% façade area, which

28

is well sheltered by the overhang. The results show that the addition of an overhang is effective in significantly reducing the WDR amount on a façade given that over 50% of WDR is deposited on the top 15% of the façade area and a typical overhang, e.g. 0.6 m overhang, can effectively shelter the top 30% façade area.

The same procedure for full overhang case is applied to the north façade and the results are shown in Table 7. Note for most of the time wind approaches the façade at an angle about 65° normal to the façade. During rain hours the dominant wind direction is from the east and there are some incidences when the wind approaches from the ENE (Fig. 8). Therefore, the distribution of wind-driven rain is not symmetrical on north façade (Fig. 12), and the assignment of catch ratio for the calculation cells is based on the actual measurements and observed wind-driven rain distribution pattern. The results shown in Table 7 are for the situation when the wind approaches the north façade at an angle. In general, the results for the north façade is very close to those found on the east façade (Table 6), within 1-3% for both overhang sizes.

Table 7. Effect of overhang on WDR reduction on the north façade (full overhang)

Façade area	No overhang		0.6 m overhang		1.2 m overhang	
	$\sum_{i=1}^{n} \eta_i A_i$	WDR distribution on façade (%)	$\sum_{i=1}^{n} \eta_i A_i$	Area-weighted effectiveness (%)	$\sum_{i=1}^{n} \eta_i A_i$	Area-weighted effectiveness (%)
A1 (15%)	1.67	35.0	0.44	73.4	0.13	92.0
A2 (30%)	2.44	50.6	0.79	67.7	0.27	89.1
A3 (60%)	3.97	82.4	1.69	57.5	0.66	83.4
A4 (100%)	4.82	100	2.53	47.4	1.51	68.0
Total WDR reduction (%)			47.4		68.6	

3.3.5 Wind speed effect

Given that wind speed and wind direction significantly influence the wetting pattern on façades, the effectiveness of overhang is analyzed with respect to wind speed and wind direction. To establish the correlation between the overhang effectiveness and wind speed, only wind with incidence angles within $\pm15^{o}$ is considered. As shown in Figure 18, there is a direct correlation between the wind speed and the percentage reduction in catch ratio for both overhang widths.

In general, the protection provided by the overhang decreases with the increase of wind speed. The 0.6 m overhang is able to significantly reduce the amount of WDR deposited on the top edge

of the facade (EN1, EN5, EN8) for low wind speeds (90 to 100%). This protection drops significantly for higher wind speeds of 2 to 4 m/s (50 to 70%) and again, albeit less drastically, for wind speeds greater than 4m/s (40 to 60%). The gauges further down the facade (EN3, EN4, EN7, EN9) receive little to no protection from the 0.6 m overhang during higher wind speeds. The 1.2 m overhang totally eliminates the WDR deposited on the top edge of the facade (EN1, EN5, EN8) for low wind speeds (100%). This protection remains significant for higher wind speeds of 2 to 4 m/s (90 to 100%) and for wind speeds greater than 4 m/s (80 to 100%). Compared to the 0.6 m overhang, for gauges further down the façade, the 1.2 m overhang remains quite effective for higher wind speeds of 2 to 4 m/s (40 to 70%) and for wind speeds greater than 4 m/s (20 to 60%). The wider overhang not only provides more direct shelter but is also more effective during periods of higher wind speeds.
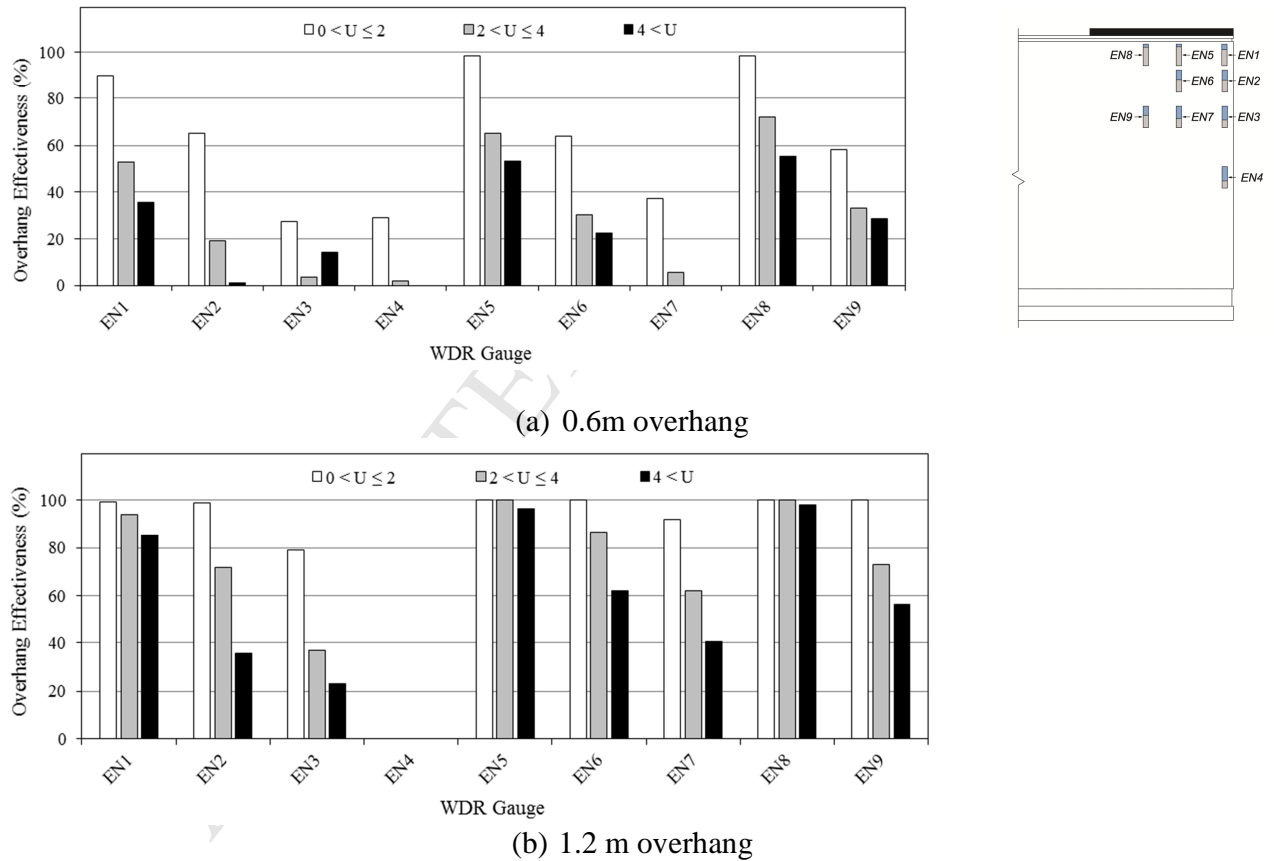

(a) 0.6m overhang

(b) 1.2 m overhang

Figure 18. Percentage reduction in catch ratio with respect to wind speed, $\theta = 0 \pm 15°$ on east façade: a) 0.6 m overhang and b) 1.2 m overhang.

3.3.6 Wind direction effect

Figure 19 shows the overhang effectiveness with respect to wind direction for gauge locations on the east façade. The following approaching wind angles towards the east facade are considered: 60° (left of the normal), 30° (left of the normal), 0° (normal to facade), and 30° (right of the normal), as shown in Figure 19. All wind speeds are considered due to the limited number of data for oblique wind angles.

a) 0.6 m overhang

Incidence wind angles towards the east facade.
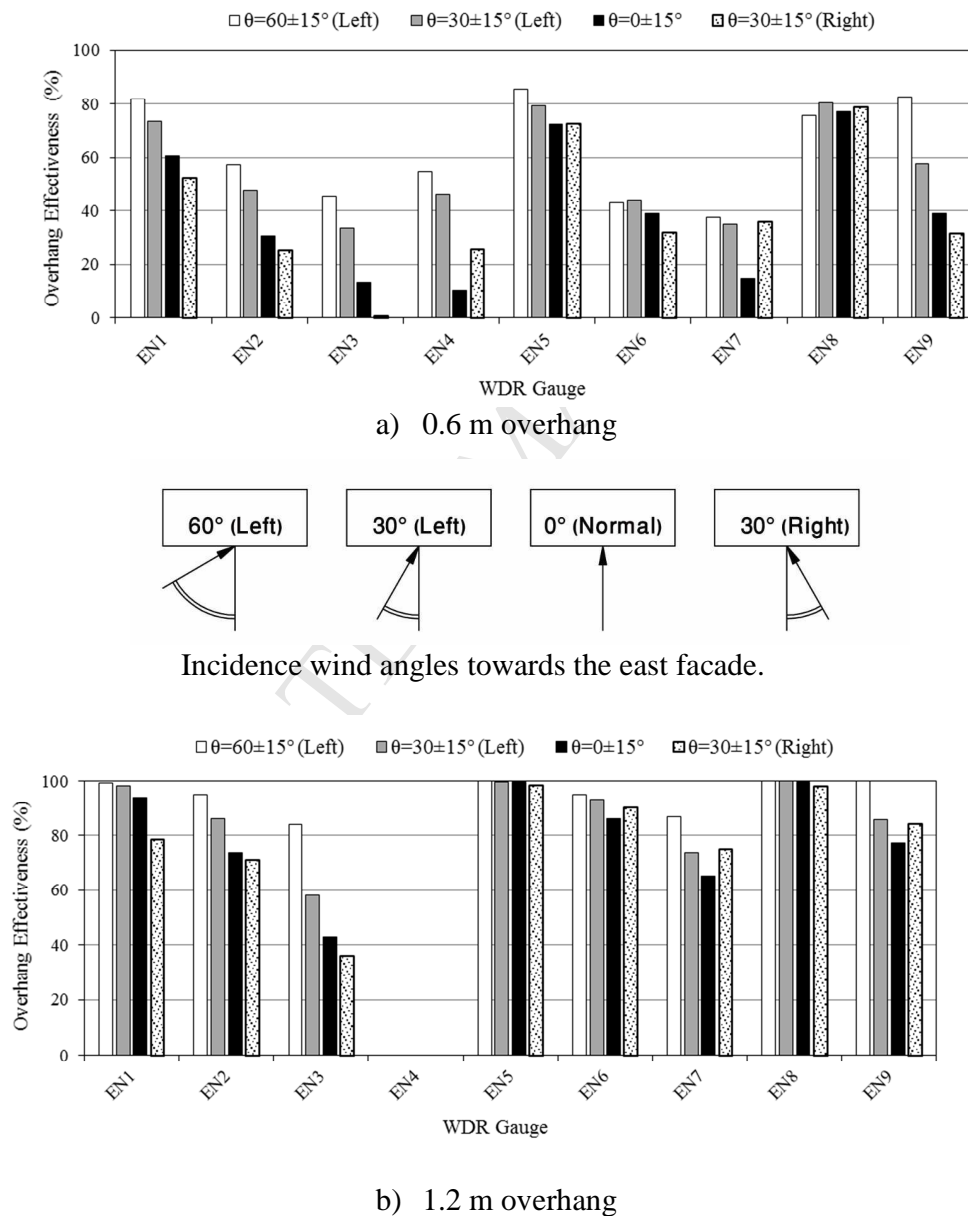

b) 1.2 m overhang

Figure 19. Overhang effectiveness with respect to wind direction: east façade: a) 0.6 m overhang and b) 1.2 m overhang. (Note: EN4 gauge was malfunction during this period).

31

The influence of wind direction on the overhang effectiveness is not as consistent as the influence of wind speed, however, a few general trends are observed.

In general, the overhang is more effective in reducing WDR for oblique winds. For the 0.6 m overhang, the significance of the wind approaching angles on the effectiveness of overhang depends on the location. For locations better protected by the overhang, the general trend is that with the increase of wind incidence angle the protection provided by the overhang increases with the least protection being for wind normal to the facade, such as the central locations EN5 and EN8. For less protected locations at the edge (EN1 to EN3), when wind coming from the southeast (left), i.e. these locations at downstream, with the increase of wind incidence angle, the protection provided by the overhang increases. For example, the effectiveness of overhang increases from 60% at incidence angle of 0±15° to 80% at incidence angle of 60±15° for EN1. However, when the wind coming from the northeast (right), i.e. these locations are at upstream, the protection decreases with the increase of incidence angle. For example, the effectiveness of overhang for EN1 is reduced from 60% at incidence angle of 0±15° to 50% when the wind incidence angle increases to 30±15° from the northeast.

The trend observed above is more consistent for the 1.2 m overhang. Locations EN5 and EN8 are fully protected by a 1.2 m overhang, therefore, the effectiveness is almost insensitive to the wind incidence angle. Locations EN6, EN7 and EN9 are better protected compared to the 0.6 m overhang, therefore, the effectiveness increases with the increase of wind incidence angle with the least protection being for wind normal to the facade. For example, the effectiveness of overhang increases from 95% at incidence angle of 0±15° to 100% at incidence angle of 60±15° for EN1. For locations at the northeast edge (EN1 to EN3), the least protected locations, the effectiveness increases with the increase of wind incidence angle for downstream wind, while the effectiveness decreases with the increase of incidence angle for upstream wind.

4. SUMMARY AND CONCLUSIONS

Although overhangs are a classical approach in protecting building facades from rain, the effectiveness of overhang in reducing WDR wetting of building facades has never been quantified. This is the first field experiment known to the authors that quantifies the effectiveness of overhang through field measurements by fitting a retractable overhang on a six-story building. This building is instrumented with a high resolution of customized WDR gauges on the façade

facing the prevailing wind direction. On-site weather data and WDR on façade have been collected over two years for three periods with and without overhang. The effectiveness of overhang, defined as the percentage reduction of catch ratios with and without overhang, is used. The effect of overhang width on WDR wetting is assessed using two methods: similarity and symmetry. The similar meteorological characteristics of wind and rain during periods with and without overhang allows the use of similar rain events to compare catch ratios with overhang to those without overhang. The predominantly easterly winds during rain results in a more or less symmetrical wetting pattern on the east façade, therefore, a symmetry approach is possible. The main findings are:

- Similarity and symmetry approaches are used and good agreement between these two approaches is obtained.

- For the particular climate in Southern British Columbia, Canada, characterized by long rainy winters with mild wind and rain, the overhang is effective and significantly reduces WDR for this six-storey building, especially for areas underneath the overhang. As expected, the larger overhang provides greater protection.

  o The effectiveness of overhang decreases when moving from the upper edge towards the ground and from the centre towards the side edge of the façade.

  o The relationship between overhang effectiveness and the distance from the roofline is quasi-linear with a smaller gradient for the 1.2 m overhang.

  o The protection area can extend to 25% of building height from the roofline for both 0.6 m and 1.2 m overhang.

  o Given that over 50% of the total amount of WDR impinged on the façade is received by the top 15% of the façade area, overhangs that can shelter the top 30% of the façade area can effectively protect the façade from WDR wetting.

- The effectiveness of overhang is influenced by wind speed and wind incidence angle. The effectiveness increases for oblique winds but decreases with the increase of wind speed.

ACKNOWLEDGEMENT

REFERENCES

[1] Kumaran, K. and Sanders, C., 2008. IEA Annex 41, Final report, Volume 3. Whole Building Heat, Air, Moisture Response - Boundary Conditions and Whole Building HAM Analysis. International Energy Agency.

[2] Blocken, B. and Carmeliet, J., 2004. A review of wind-driven rain research in building science. Journal of Wind Engineering and Industrial Aerodynamics; 92 (13): 1079-1130.

[3] Boyd, D.W. 1963. Driving rain map of Canada. *Technical Note No. 398.* Division of Building Research, National Research Council of Canada, Ottawa.

[4] Lacy RE, 1965. Driving rain maps and the onslaught of rain on buildings. RILEM/CIB Symposium on Moisture Problems in Buildings, Rain Penetration. Helsinki, Aug. 16-19. Vol. 3: 3-4.

[5] Fazio, P., Mallidi, S.R. and Zhu, D., 1995. A quantitative study for the measurement of driving rain exposure in Montreal region. Building and Environment; 30(1): 1-11.

[6] Zhu, D., Mallidi, S. R., and Fazio, P., 1995. Quantitative driving rain exposure on a vertical wall at various Canadian cities. Building and Environment; 30(4):533-544.

[7] Straube J. and Burnett E. 1997. Driving rain and masonry veneer. ASTM Symposium on Water Leakage Through Building Facades, Orlando, March 17 1996. Special Technical Publication, ASTM STP 1314, Philadelphia, 73-87.

[8] Straube, J. and Burnett, E., 2000. Simplified prediction of driving rain on buildings. *Proceedings of the International Building Physics Conference*, Eindhoven University of Technology, Eindhoven, the Netherlands, pp. 375-382.

[9] Choi ECC. 1993. Simulation of wind-driven rain around a building. Journal of Wind Engineering and Industrial Aerodynamics; 46:721-729.

[10] Choi, E. C. (1999). Wind-driven rain on building faces and the driving-rain index. Journal of Wind Engineering and Industrial Aerodynamics; 79(1):105-122.

[11] Choi, E. C. (2000). Variation of wind-driven rain intensity with building orientation. Journal of Architectural Engineering; 6(4):122-128.

[12] Hangan, H. 1999. Wind-driven rain studies. A C-FD-E approach. Journal of Wind Engineering and Industrial Aerodynamics; 81:323-331.

[13] Blocken, B. and Carmeliet, J., 2006. Validation of CFD simulations of wind-driven rain on a low-rise building façade. Building and Environment; 42(7):2530-2548.

[14] Abuku M, Blocken B, Nore K, Thue JV, Carmeliet J, Roels S., 2009. On the validity of numerical wind-driven rain simulation on a rectangular low-rise building under various oblique winds. Build and Environment; 44(3): 621-632.

[15] Huang, S. H., and Li, Q.S. 2010. Numerical simulations of wind-driven rain on building envelopes based on Eulerian multiphase model. Journal of Wind Engineering and Industrial Aerodynamics; 98(12): 843-857.

[16] Kubilay, A., Derome, D, and Blocken, B. 2013. CFD simulation and validation of wind-driven rain on a building facade with an Eulerian multiphase model. Building and Environment. 61: 69-81.

[17] Kubilay, A., D. Derome, B. Blocken, and J. Carmeliet. 2014. Numerical simulations of wind-driven rain on an array of low-rise cubic buildings and validation by field measurements. Building and Environment. 81:283-295.

[18] Pettersson, K., S. Krajnovic, A.S. Kalagasidis and P. Johansson. 2016. Simulating wind-driven rain on building facades using Eulerian multiphase with rain phase turbulence model. Building and Environment 106: 1-9.

[19] Kubilay, A., D. Derome, and J. Carmeliet, 2017. Analysis of time-resolved wind-driven rain on an array of low-rise cubic buildings using large eddy simulation and an Eulerian multiphase model. Building and Environment. 114: 68-81.

[20] Derome, D., A. Kubilay, T. Defraeve, B. Blocken and J. Carmeliet. 2017. Ten questions concerning modeling of wind-driven rain in the built environment. Building and Environment 114:495-506.

[21] Blocken B. and Carmeliet, J. 2005. High-resolution wind-driven rain measurements on a low-rise building—experimental data for model development and model validation. Journal of Wind Engineering and Industrial Aerodynamics; 93(12): 905–928.

[22] Nore, K., Blocken, B., Petter Jelle, B., Thue, J.V., and Carmeliet, J., 2007. A dataset of wind-driven rain measurements on a low-rise test building in Norway. Building and Environment. 42(5):2150-2165.

[23] Kubilay A, Derome D, Blocken B, and Carmeliet J., 2014. High-resolution field measurements of wind-driven rain on an array of low-rise cubic buildings. Building and Environment. 78: 1-13.

[24] Deb Nath, K. U., V., Chiu, and H. Ge. Measurements of wind-driven rain on mid- and high-rise buildings in three Canadian regions. Proceedings of the 6th International Building Physics Conference: Building Physics for a Sustainable Built Environment. Turin, Italy. June 14-17, 2015.

[25] Blocken B. and Carmeliet, J. 2002. Spatial and temporal distribution of driving rain on a low-rise building. Wind and Structures 5(5):441-462.

[26] Blocken B. and Carmeliet J. 2006. The influence of the wind-blocking effect by a building on its wind-driven rain exposure. J. of Wind Engineering and Industrial Aerodynamics; 94: 101-127.

[27] Blocken, B., Dezsö, G., Beeck, J. V., and Carmeliet, J., 2009. The mutual influence of two buildings on their wind-driven rain exposure and comments on the obstruction factor. Journal of Wind Engineering and Industrial Aerodynamics; 31: 1-21.

[28] Blocken, B. and Carmeliet, J., 2010. Overview of three state-of-the-art wind-driven rain assessment models and comparison based on model theory. Building and Environment. 45(3): 691-703.

[29] Blocken, B., Abuku, M., Nore, K., Briggen, P. M., Schellen, H. L., Thue, J. V., Roels, S., and Carmeliet, J., 2011. Inter-comparison of wind-driven rain deposition models based on two case studies with full-scale measurements. Journal of Wind Engineering and Industrial Aerodynamics; 99(4): 448-459.

[30] Foroushani, S., Ge, H. and Naylor, D. 2013. Effects of roof overhangs on wind-driven rain wetting of a low-rise cubic building: a numerical study. Journal of Wind Engineering and Industrial Aerodynamics; 125: 38-51.

[31] Kubilay, K., D. Derome, B. Blocken, and J. Carmeliet. 2015. Wind-driven rain on two parallel wide buildings: field measurements and CFD simulations, J. Wind Eng. Ind. Aerod 146:11-28.

[32] Kubilay, A., Carmeliet J. and Derome, D. 2017. Computational fluid dynamics simulations of wind-driven rain on a mid-rise residential building with various types of façade details. Journal of Building Performance Simulation; 10 (2): 125-143.

[33] Lakehal, D., Mestayer, P.G., Edson, J.B., Anquetin, S., and Sini, J.E. 1995. Eulero-Lagarangian simulation of raindrop trajectories and impacts within the urban canopy. Atmos. Environ. 29(23):3501-3517.

[34] Etyemezian, V., C.I. Davidson, M. Zufall, W. Dai, S. Finger, M. Striegel. 2000. Impingement of rani drops on a tall building. Atmos. Environ. 34:2399-2412.

[35] Briggen, P.M., B. Blocken and H.I. Schellen. 2009. Wind-driven rain on the façade of a monumental tower: numerical simulation, full-scale validation and sensitivity analysis. Build. Environ. 44 (8):1675-1690.

[36] Kubilay, A., D. Derome, B. Blocken, and J. Carmeliet. 2015. Numerical modeling of turbulent dispersion for wind-driven rain on building facades, Environ. Fluid Mech. 15 (1):109-133.

[37] Inculet, D. and Surry, D. 1995. Simulation of wind-driven rain and wetting patterns on buildings. Research report for Canadian Mortgage and Housing Corporation, Ottawa.

[38] Hershfield, Morrison, 1996. Survey of building envelope failures in the coastal climate of British Columbia. Canadian Mortgage and Housing Corportion, Ottawa.

[39] Ge, H. and Krpan, R. 2009. Wind-driven rain study in the Coastal Climate of British Columbia. Research report submitted to Canadian Mortgage and Housing Corporation, Ottawa. https://www.bchousing.org/publications/**WindDrivenRainStudy**.pdf

[40] Chiu, V. 2016. The effect of overhang on wind-driven rain wetting of a mid-rise building. M.A.Sc thesis. Concordia University, Montreal, Canada.

[41] International Standard Organization (ISO). Hygrothermal performance of buildings-Calculation and presentation of climatic data—part 3: Calculation of a driving rain index for vertical surfaces from hourly wind and rain data. ISO 15927-3:2009.

Highlights:

- Effectiveness of overhang on reducing WDR wetting of a six-story building is quantified by field measurements

- Similarity and symmetry approaches used to evaluate the effectiveness of overhang show good agreement

- Larger overhangs provide greater protection and protection increases from the side edge to the center and from the bottom to the top of the façade

- The relationship between overhang effectiveness and distance from the roofline is quasi-linear with smaller gradient for the larger overhang

- Effectiveness of overhang increases for oblique winds but decreases with the increase of wind speed